

## Chapter 3

# Principles of Ultrasonic Propagation

The principles upon which ultrasonic sensing of solidification processes is founded are beginning to become well established. The concepts underlying of ultrasonic wave propagation in liquids and solids and the interactions of these waves with solid-liquid interfaces are reviewed below together with ultrasonic ray theory. Emerging laser methods for conducting ultrasonics (*i.e.* laser generation and detection of ultrasound) are then examined.

### 3.1 Ultrasonic Wave Propagation

Ultrasonic disturbances of small amplitude propagate as linear elastic waves whose propagation through a body results in particle oscillations about their equilibrium positions. In ideal liquids and gases only one propagation mode exists. This longitudinal mode has particle displacements parallel to the direction of ultrasonic propagation. The ultrasonic velocity is governed by the materials compressibility and for these materials, is independent of propagation direction. Elastic solids can accommodate transverse waves (where particle displacements are perpendicular to the direction of propagation) as well as

longitudinal waves. The particle motions in elastic solids associated with these three bulk modes of propagation can be resolved into three perpendicular components, one longitudinal and two transverse to the direction of propagation. The theory of linear elastic wave propagation in both liquids [84,85] and solids [86-88] have been widely reviewed. A brief review of wave propagation principles applicable to laser ultrasonic sensing is presented below.

### 3.1.1 Wave Propagation in Liquids

When an ultrasonic wave propagates through a liquid the density, pressure and temperature of an infinitesimal element of liquid vary periodically with time. In ideal (non-viscous, non-absorbing) liquids, the pressure/density cycle due to propagation of an ultrasonic wave takes place adiabatically or at constant entropy [84,85]. With these assumptions a plane harmonic wave (*i.e.* longitudinal wave) propagates unattenuated and with a frequency independent velocity that is determined by the liquids compressibility from the thermodynamic equations of state [85].

In the case of non-ideal liquids, the liquid may exhibit either viscous or absorption effects, *i.e.* some of the ultrasonic energy is dissipated (by local heating) and the wave attenuates in amplitude with propagation. In this case the ultrasonic velocity becomes frequency dependent (dispersive propagation). This non-ideal wave propagation can be described by Navier-Stokes equation of hydrodynamics (in the acoustic approximation):

$$\rho_o \frac{\partial^2 \mathbf{u}(x,t)}{\partial t^2} = \rho_o \left( \frac{\delta P}{\delta \rho} \right) \frac{\partial^2 \mathbf{u}(x,t)}{\partial x^2} + \left( b + \frac{4}{3} \eta \right) \frac{\partial}{\partial t} \left( \frac{\partial^2 \mathbf{u}(x,t)}{\partial x^2} \right) \quad (3.1)$$

where  $\mathbf{u}(x,t)$  is the particle velocity,  $\rho_o$  is the density of the liquid in the absence of the sound wave,  $\delta P$  and  $\delta \rho$  are the changes in the pressure and density due to  $\mathbf{u}(x,t)$ ,  $b$  is the

bulk or volume viscosity and  $\eta$  is the dynamic or shear viscosity [85]. Assuming one-dimensional plane harmonic wave propagation ( $u_1$  is a function of  $x_1$  only,  $u_2 = u_3 = 0$ ),  $\delta P/\delta\rho = K_S/\rho_o$  where  $K_S$  is the adiabatic bulk modulus. By defining a characteristic frequency  $\omega_v = K_S(b + (4/3)\eta)^{-1}$  a dispersion equation may be expressed as

$$k^2 = \omega^2 \left( \frac{\rho_o}{K_S} \right) \frac{1}{1 + i\omega/\omega_v}. \quad (3.2)$$

Since  $\omega$  is real,  $k$  can take complex values,  $k = k_1 - ik_2$ , where  $k_1$  and  $k_2$  are both real and positive, and solving for a plane wave propagating in the  $x_1$ -direction, the longitudinal wave phase velocity can be expressed in the form:

$$v = \frac{\omega}{k_1} = \sqrt{\frac{2K_S}{\rho_o} \frac{[1 + (\omega/\omega_v)^2]}{1 + [1 + (\omega/\omega_v)^2]^{1/2}}}, \quad (3.3)$$

where the *amplitude attenuation per wavelength* can be expressed as:

$$\alpha = \frac{2\pi vk_2}{\omega} = \pi \left( \frac{v^2 \rho_o}{K_S} \right) \frac{\omega/\omega_v}{1 + (\omega/\omega_v)^2}. \quad (3.4)$$

As  $b$  and  $\eta \rightarrow 0$  and/or  $\omega \ll \omega_v$  (*i.e.* MHz region for non-viscous liquids), the longitudinal wave phase velocity,  $v_{liq}$ , approaches that of an ideal liquid and is given by

$$v_{liq} = \sqrt{\frac{K_S}{\rho}}. \quad (3.5)$$

As an initial assumption  $b$  is allowed to approach zero and viscous effects are due to  $\eta$  only [88]. Substituting values of  $K_S = 10.17$  GPa and  $\eta = 2.5$  cp for liquid  $\text{Cd}_{0.96}\text{Zn}_{0.04}\text{Te}$  at  $1100^\circ\text{C}$  into  $\omega_v = K_S(b + (4/3)\eta)^{-1}$ , the characteristic frequency is

approximately 300 GHz. Figures 3.1 and 3.2 show the deviation from ideality (Eqns. (3.5) and (3.6)) for the longitudinal wave phase velocity and the *amplitude attenuation per wavelength* for liquid  $\text{Cd}_{0.96}\text{Zn}_{0.04}\text{Te}$  at  $1100^\circ\text{C}$  as the normalized frequency  $\omega/\omega_v$  is increased. It is clear from Fig. 3.1 that the range of frequencies generated from laser based ultrasonics ( $< 3$  MHz) falls in the linear portion of the curve. Therefore ideal behavior is assumed and the longitudinal wave phase velocity does not deviate from Eqn. (3.5). Although the *amplitude attenuation per wavelength* does deviate from ideality in this range of frequencies, the attenuation is small until the frequency exceeds 3 GHz.

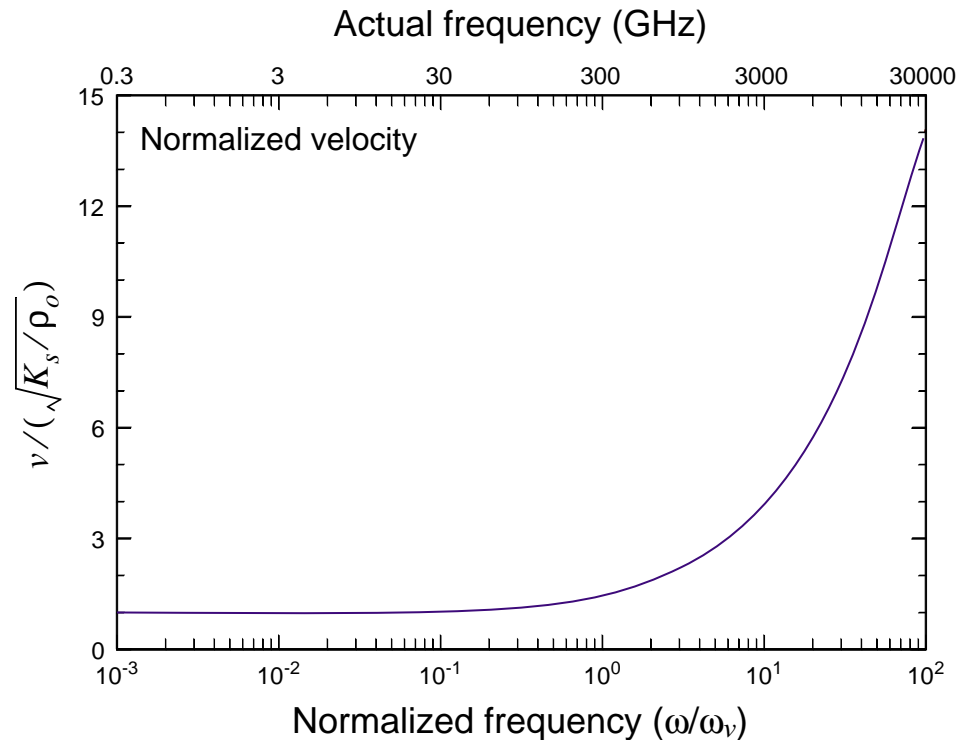


**Figure 3.1** The deviation from ideality of the longitudinal wave phase velocity vs. the normalized frequency for liquid  $\text{Cd}_{0.96}\text{Zn}_{0.04}\text{Te}$  at  $1100^\circ\text{C}$ .

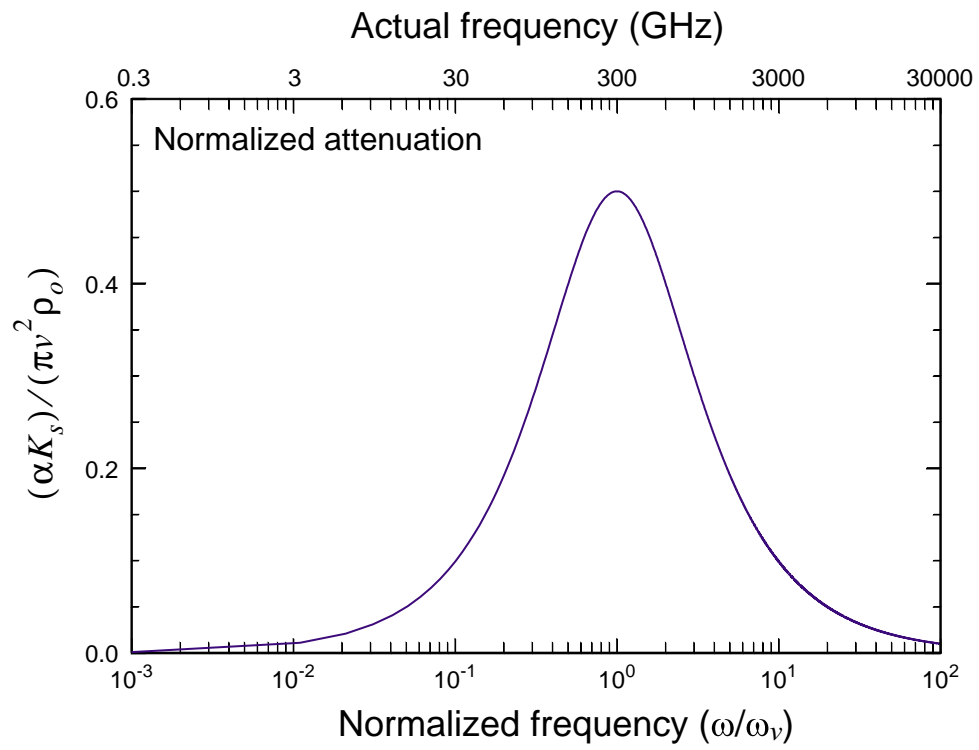


**Figure 3.2** The deviation from ideality of the *amplitude attenuation per wavelength* vs. the normalized frequency for liquid  $\text{Cd}_{0.96}\text{Zn}_{0.04}\text{Te}$  at  $1100^\circ\text{C}$ .

### 3.1.2 Wave Propagation in Solids

In elastic solids each of the three modes has its own characteristic velocity, although in isotropic solids the two transverse velocities are degenerate. For anisotropic solids the phase velocity ( $v$ ) of the three possible bulk wave modes (quasi-longitudinal, fast and slow quasi-shear) in a direction defined by the unit propagation vector,  $\mathbf{n}$ , with components  $n_j$ ,  $j = 1,2,3$  can be found from the eigenvalues of the Christoffel equation [88]:

$$(k^2 c_{ijkl} n_k n_l - \rho \omega^2 \delta_{ij}) d_j = 0, \quad i = 1,2,3 \quad (3.6)$$

where  $\rho$  is the density,  $k = \omega/v$  is the wave number,  $\omega$  is the angular frequency,  $c_{ijkl}$  are the components of the elastic stiffness tensor,  $d_j$ ,  $j = 1,2,3$  are the components of the unit particle displacement vector,  $\mathbf{d}$ , and  $\delta_{ij}$  is the Kronecker delta [88]. For a given propagation direction vector  $\mathbf{n}$ , the squares of the phase velocities of the bulk modes are obtained as the eigenvalues of Eqn. (3.6). The particle displacement vector  $\mathbf{d}$  of a bulk mode is obtained as a unit eigenvector for the phase velocity (eigenvalue) of the bulk mode. The slowness (or inverse velocity) surface gives the inverse phase velocity as a function of propagation direction and is independent of  $\omega$ . Some useful properties of the slowness surface are examined below.

An important consequence of anisotropic wave propagation is that the energy of a wave packet does not necessarily propagate parallel to the wave propagation direction [88]. In a lossless medium, the energy<sup>1</sup> or group velocity is perpendicular to the slowness surface. The power flow angle (defined as the angle between the energy velocity and the propagation direction,  $k$ ) depends on the shape of the slowness surface and therefore

---

1. It is assumed that waves propagate in a lossless medium and the terms energy and group velocity are therefore used interchangeably.

changes with crystallographic orientation. The group velocity, which governs the speed of a modulated disturbance (*i.e.* a pulse), can be determined once the phase velocity and the displacement vector for a specific mode are known. The Cartesian components of the group velocity,  $v_g$ , are then obtained from [88]

$$v_{g_i} = \frac{c_{ijkl}d_j d_l n_k}{\rho v}, \quad i = 1,2,3. \quad (3.7)$$

Equation (3.7) may be greatly simplified for propagation in high-symmetry directions, where the phase and group velocities are equal [88].

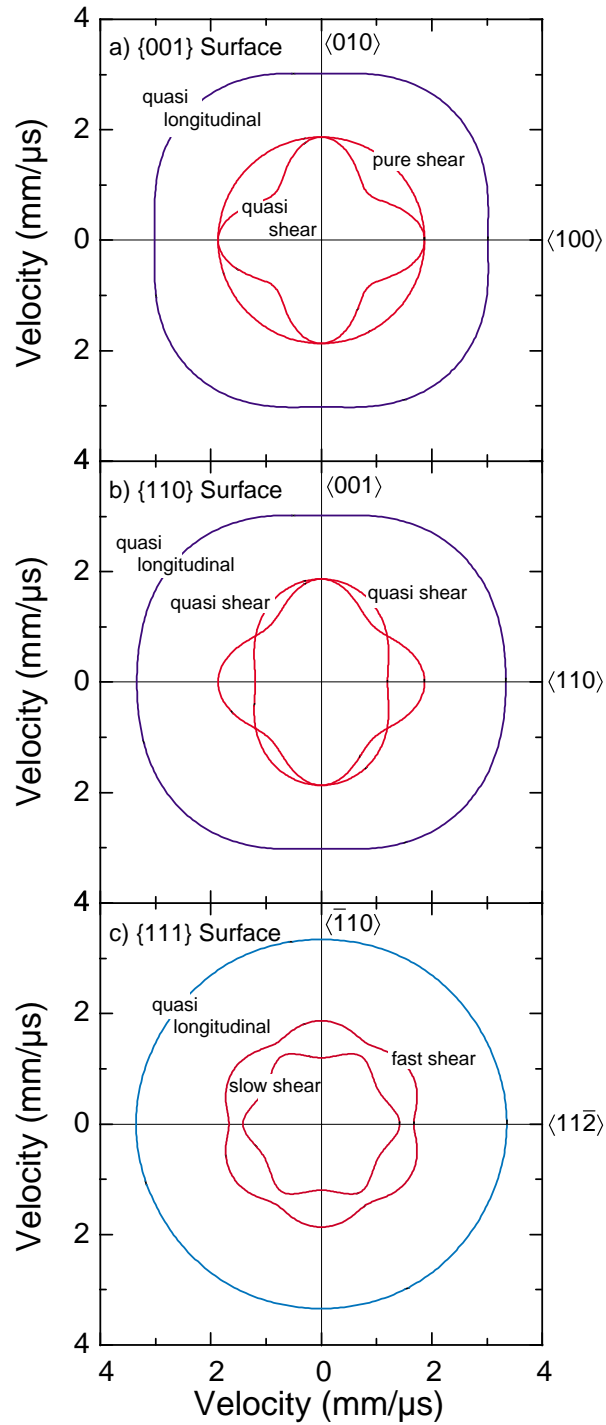
The most straight forward and precise method for evaluating the elastic stiffness constants of anisotropic solids is through the measurement of the ultrasonic velocity of pure longitudinal and pure shear modes propagating in principal symmetry directions, *i.e.* in the  $\langle 100 \rangle$ ,  $\langle 110 \rangle$  and  $\langle 111 \rangle$  for cubic materials. Cadmium telluride and its substitutional solid solution (Cd,Zn)Te alloys crystallize in a zinc-blende (cubic) structure. It can be shown from Eqn. (3.6) and (3.7) that the three bulk wave velocities (one longitudinal and two shear) can be expressed as a function of the elastic stiffness constants  $C_{11}$ ,  $C_{12}$ ,  $C_{44}$  and the density  $\rho$ . Table 3.1 gives the expressions for the pure longitudinal and pure shear velocities in the primary  $\langle 100 \rangle$ ,  $\langle 110 \rangle$  and  $\langle 111 \rangle$  directions for a cubic crystal structure. Note, that the two shear wave velocities are equivalent in both  $\langle 100 \rangle$  and  $\langle 111 \rangle$  directions. Moreover, it can be shown that in all cases in Table 3.1, except for the shear wave in the  $\langle 111 \rangle$  direction, the energy flux vector is in the same direction as the wave normal [88].

Table 3.1: Relationships between elastic constants and ultrasonic velocities for cubic materials.

Direction of Wave Propagation	Direction of Particle Motion	Type of Wave	Velocity
$\langle 100 \rangle$	$\langle 100 \rangle$	Longitudinal	$V_l = \sqrt{\frac{C_{11}}{\rho}}$
$\langle 100 \rangle$	in plane $(100)$	Shear	$V_s = \sqrt{\frac{C_{44}}{\rho}}$
$\langle 110 \rangle$	$\langle 110 \rangle$	Longitudinal	$V_l = \sqrt{\frac{C_{11} + C_{12} + 2C_{44}}{2\rho}}$
$\langle 110 \rangle$	$\langle 001 \rangle$	Shear (fast shear)	$V_{fs} = \sqrt{\frac{C_{44}}{\rho}}$
$\langle 110 \rangle$	$\langle \bar{1}\bar{1}0 \rangle$	Shear (slow shear)	$V_{ss} = \sqrt{\frac{C_{11} - C_{12}}{2\rho}}$
$\langle 111 \rangle$	$\langle 111 \rangle$	Longitudinal	$V_l = \sqrt{\frac{C_{11} + 2C_{12} + 4C_{44}}{3\rho}}$
$\langle 111 \rangle$	in plane $(111)$	Shear	$V_s = \sqrt{\frac{C_{11} - C_{12} + C_{44}}{3\rho}}$

Velikov and Rusakov [89] report that cadmium telluride (a cubic crystal) has three independent elastic stiffness constants:  $C_{11} = 53.30$  GPa,  $C_{12} = 36.50$  GPa and  $C_{44} = 20.44$  GPa while the density equals  $5.854$  g/cm<sup>3</sup> at 20°C [90]. Bulk cubic single-crystal materials for electronic applications are usually grown with a low index crystallographic orientation such as  $\langle 100 \rangle$ ,  $\langle 110 \rangle$  or  $\langle 111 \rangle$ . Using the elastic constants of Vekilov and Rusakov, Figs. 3.3 - 3.5 show the calculated phase velocity, slowness and group velocity surfaces for the three bulk modes on the  $\{001\}$ ,  $\{110\}$  and  $\{111\}$  planes of CdTe, respectively.

On the  $\{001\}$  planes the quasi-longitudinal group velocity is greatest in  $\langle 110 \rangle$  directions and the smallest in  $\langle 100 \rangle$  directions. On  $\{110\}$  planes the velocity is greatest in  $\langle 111 \rangle$  direction and smallest in  $\langle 001 \rangle$  directions; minimal anisotropy is present on the  $\{111\}$  plane for the quasi-longitudinal mode. The cusps on the quasi-shear curves of Fig. 3.5 arise from the convoluted form of the quasi-shear slowness curve, Fig. 3.4, on the vicinity of high symmetry directions [88]. This is due to the fact that there are two wave vectors (near the vicinity of each high symmetry direction) that correspond to energy flow along the high symmetry direction. It follows that these two wave vectors must have the same energy velocity as the wave propagating in the high symmetry direction. No cusps are observed for the pure shear mode of Fig. 3.5(a) because the slowness surface is a sphere and the energy or group velocity is parallel to the wave propagation direction,  $k$ . Details of the algorithm developed to solve for the phase and group velocities can be found in Appendix A.



**Figure 3.3** Phase velocity surfaces for cadmium telluride on the (a) {001}, (b) {110}, and (c) {111} planes assuming  $C_{11} = 53.30$  GPa,  $C_{12} = 36.50$  GPa,  $C_{44} = 20.44$  GPa and  $\rho = 5.854$  g/cm<sup>3</sup> at 20°C.

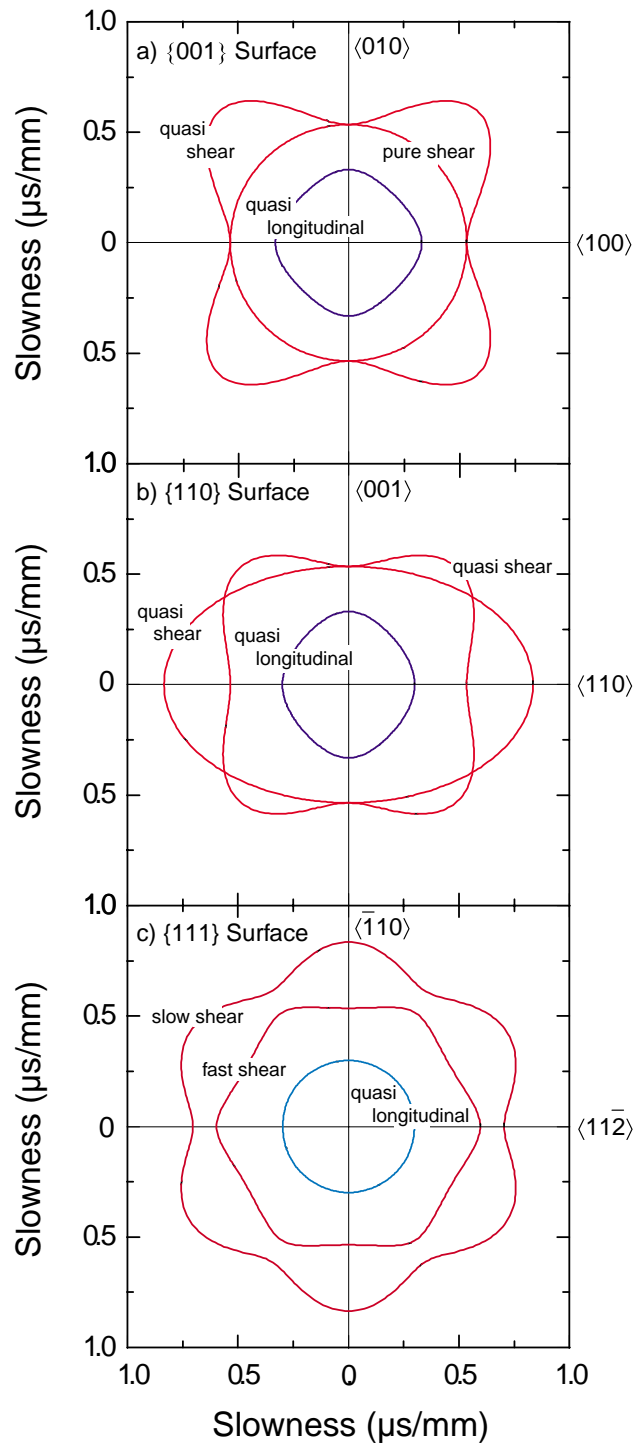


**Figure 3.4** Slowness surfaces for cadmium telluride on the (a)  $\{001\}$ , (b)  $\{110\}$ , and (c)  $\{111\}$  planes assuming  $C_{11} = 53.30$  GPa,  $C_{12} = 36.50$  GPa,  $C_{44} = 20.44$  GPa and  $\rho = 5.854$  g/cm<sup>3</sup> at 20°C.

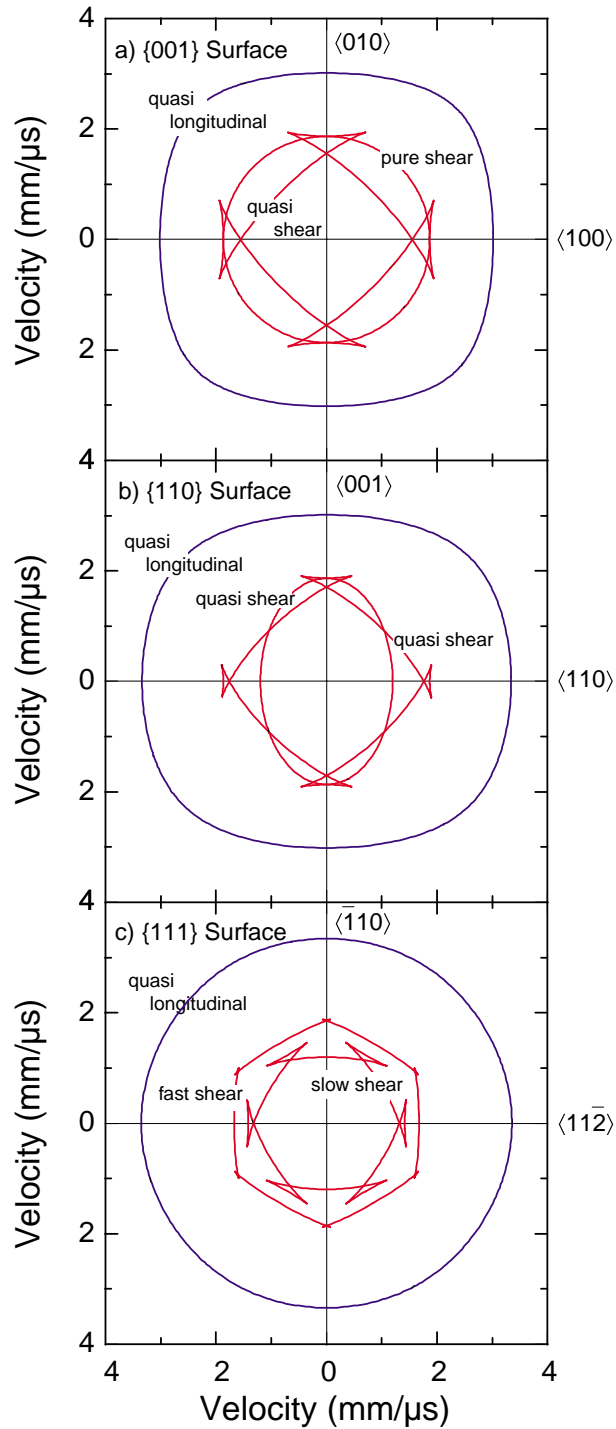


**Figure 3.5** Group velocity surfaces for cadmium telluride on the (a) {001}, (b) {110}, and (c) {111} planes assuming  $C_{11} = 53.30$  GPa,  $C_{12} = 36.50$  GPa,  $C_{44} = 20.44$  GPa and  $\rho = 5.854$  g/cm<sup>3</sup> at 20°C.

### 3.2 Reflection/Transmission at a Liquid-Solid Interface

When an ultrasonic wave propagating in a homogeneous medium passes through an interface at a normal incident angle where the velocity (*i.e.* elastic stiffness and density) of the second medium is different (*i.e.* solid-solid or solid-liquid interface) the incident wave is reflected and transmitted with out any change in propagation direction. However when an ultrasonic wave propagating in a homogeneous medium passes through an interface at a non normal incident angle the incident wave is mode converted (a change in the nature of the wave motion) and refracted (a change in direction of wave propagation) [91-95]. These phenomena may affect the entire beam or only a portion of the beam and the sum total of the changes that occur at the interface depends on the angle of incidence and the velocity of the ultrasonic waves leaving the point of impingement on the interface [79]. Figure 3.6 shows a diagram of the relationship of possible reflected and refracted waves of an incident longitudinal wave in a liquid impingent on a solid interface.

The reflection and refraction of these ultrasonic waves is governed by the acoustic analog of Snell's law (the ratio of the sine of the angle of incidence to the sine of the angle of reflection or refraction equals the ratio of the corresponding wave velocities):

$$\frac{\sin \theta_{liq}}{v_{liq}} = \frac{\sin \theta_l}{v_l} = \frac{\sin \theta_s}{v_s} = \frac{\sin \theta_{head}}{v_{head}} \quad (3.8)$$

where  $\theta_{liq}$ ,  $\theta_l$ ,  $\theta_s$  and  $\theta_{head}$  are the ray propagation angles (with respect to the surface normal) and  $v_{liq}$ ,  $v_l$ ,  $v_s$  and  $v_{head}$  are the velocities of the longitudinal wave in the liquid, the longitudinal, shear and the head wave<sup>1</sup> in the solid.

---

1. A head wave is an wave which propagates at a liquid - solid interface.

Referring to Fig. 3.6, if the angle of incidence,  $\theta_{\text{liq}}$ , is small, the incident wave undergoes a mode conversion at the liquid-solid interface, resulting in the simultaneous propagation of longitudinal and shear waves in the solid. If the angle  $\theta_{\text{liq}}$  is increased, the direction of the refracted longitudinal wave will approach the plane of the liquid-solid interface,  $\theta_{\text{long}} \rightarrow 90^\circ$ . At the first critical incident angle,  $\theta_{\text{long}} = 90^\circ$  and the refracted longitudinal wave will disappear, leaving only a refracted (mode converted) shear wave to propagate in the solid. If  $\theta_{\text{liq}}$  is increased beyond this first critical angle, the direction of the refracted shear wave will approach the plane of the liquid-solid interface,  $\theta_{\text{shear}} \rightarrow 90^\circ$ . At this second critical incident angle,  $\theta_{\text{shear}} = 90^\circ$  and the refracted shear wave will disappear and the incident wave is only reflected at an angle equal to the incident angle. This methodology can be applied to any interface (*i.e.* liquid-solid, solid-liquid, solid-solid).

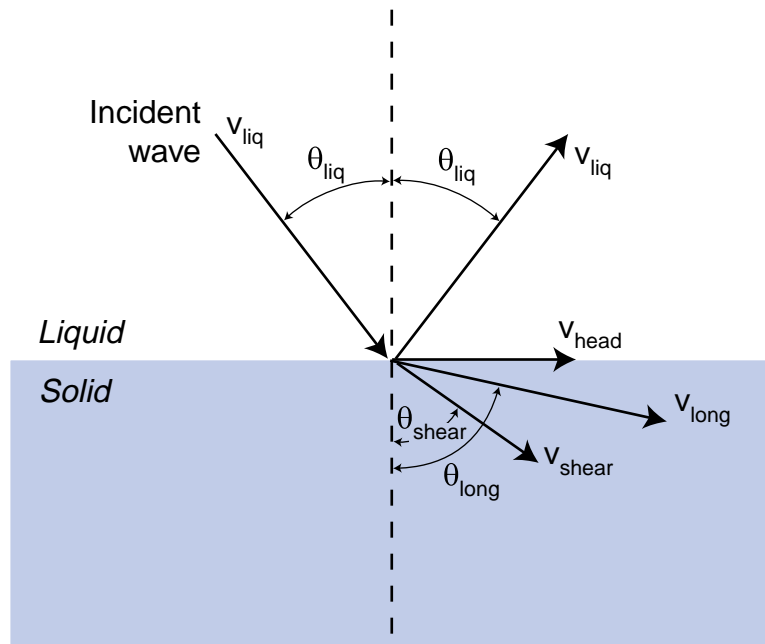


**Figure 3.6** A schematic illustration showing reflected, refracted and mode converted rays at a liquid-solid interface.

### 3.3 Ultrasonic Ray Theory/ Image Reconstruction

#### 3.3.1 Ultrasonic Ray Theory

Geometrical acoustics or ray theory describes the propagation behavior of acoustic rays in liquid and solid bodies. In the development of an ultrasonic sensor methodology for reliable image reconstruction using refracted ray paths, the sometimes severe nature of ray bending implies a need for precise knowledge of ray paths if TOF data is to be used for image reconstruction. At the fundamental level, the measured time-of-flight,  $\tau_m$ , for an acoustic ray that propagates along a path of length  $L_m$  is defined by

$$\tau_m = \int_{L_m} \frac{dl}{v}, \quad m = 1, 2, \dots, M \quad (3.9)$$

where  $dl$  is an infinitesimal element of the path,  $v$  is the ultrasonic velocity ( $1/v$  is the local slowness) within the object and  $M$  is the number of different rays.

In general there are two methods for determining the ray path between two points; shooting and bending. The shooting method uses an iterative procedure to determine the ray path from the source point by solving the differential equations that follow from ray theory for different initial conditions until the ray arrives at the receiver point [96-98]. Ray bending uses Fermat's principle as a starting point; it tries to determine a ray path between two points by searching for the minimum travel-time between them [96-98].

Both methods have serious limitations. By shooting a fan of rays leaving the source, one can obtain an impression of the wave field. However, convergence problems are known to occur frequently, especially in three-dimensions. Also, shooting will not find diffracted ray paths or ray paths in shadow zones, where ray theory breaks down. With bending, one can find every ray path satisfying Fermat's principle, even a diffracted one,

but only for one source-receiver pair at a time, and it is not certain whether the path has an absolute minimum travel-time or only a local minimum travel-time. The reader is referred to several comprehensive reviews on ray theory and ray tracing in isotropic and anisotropic materials by Moser [96-98], Andersen *et al.* [99] and Kline and Wang [100,101]. For the work contained within, both shooting and ray bending methods were used.

### 3.3.2 Image Reconstruction

Ultrasonic computerized tomography (CT) has been widely used in the fields of seismology and medicine. However, it has been finding recent applications in non destructive testing applications. It has been shown, Eqn. (3.9), that the time of flight of an individual ray path or raysum is the path integral of the ultrasonic slowness. A set of either parallel or fan-beam raysums encompassing an image is called a projection, Fig. 3.7. To reconstruct an object image from ultrasonic TOF projection data either convolution back-projection (CB) methods or algebraic reconstruction techniques (ART) are generally utilized [102,103].

Convolution backprojection methods have not been applied to situations where ray bending is significant, and although algebraic reconstruction techniques are beginning to incorporate ray bending [104], both these procedures require large data sets which may be difficult to obtain during crystal growth. Reconstruction approaches that can be used with limited data and exploit the often significant *a priori* information available are preferable.

The crystal grower requires only the axial location of the interface (its change with time gives the solidification velocity) and its approximate curvature. If the liquid and solid velocities could be also obtained, they might also be useful since they are related to the local temperature, composition and the crystals crystallographic orientation.

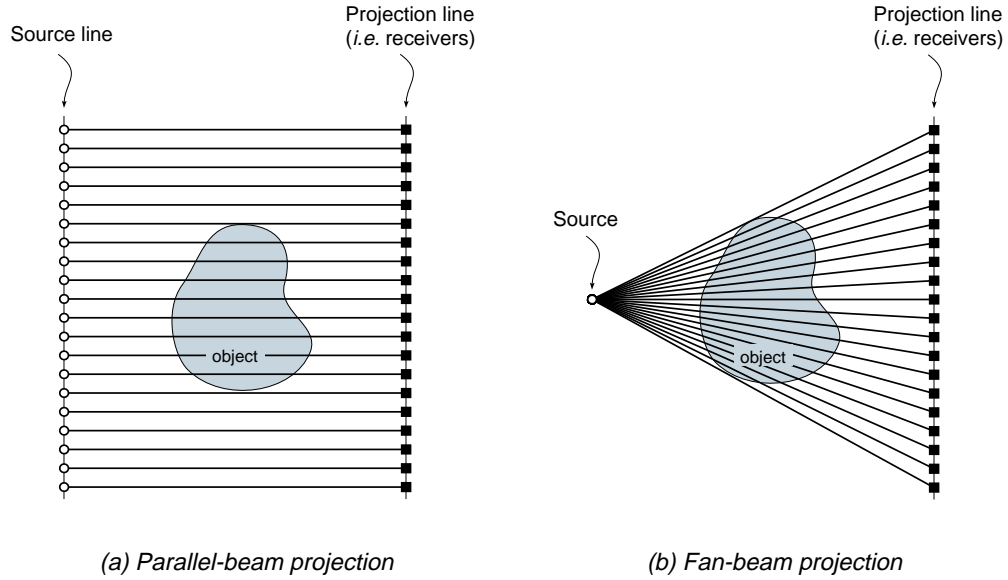


**Figure 3.7** A schematic illustration showing a) parallel beam and b) fan beam projections, assuming no ray bending.

From this, an interface model can be constructed and a nonlinear least squares reconstruction approach can be applied for image reconstruction using ultrasonic TOF projection data.

In general, a nonlinear least squares reconstruction approach calculates an initial TOF projection set from the model's trial solution and proceeds until the  $\chi^2$  merit function stops or effectively stops decreasing. If the model to be fitted is represented by  $\hat{\tau}_i = \hat{\tau}(x_i, \mathbf{a})$  then the  $\chi^2$  merit function can be expressed by

$$\chi^2(\mathbf{a}) = \sum_{i=1}^M \left[ \frac{\tau_i - \hat{\tau}(x_i, \mathbf{a})}{\sigma_i} \right]^2 \quad (3.10)$$

where  $\tau_i$  are the measured TOFs and  $\hat{\tau}_i$  are the numerically simulated TOF's for each iteration,  $M$  is the number of data points and  $\mathbf{a}$  is the matrix notation of the unknown parameters.

ters [105]. If the uncertainty ( $\sigma$ ) is unknown, as in this case, then it is assumed constant and equal to 1.

### 3.4 Laser Ultrasonics

Laser based ultrasonics, as described here, refers to laser generation and laser interferometric detection of ultrasound. In general, laser generation of ultrasound is based on the absorption of electromagnetic (light) energy and its conversion to acoustic (mechanical) energy. The laser ultrasonic approach emerged after the development of  $Q$ -switched lasers which allow the rapid deposition of significant electromagnetic energy on a surface and the resultant production of energetic elastic waves (ultrasound). Most laser ultrasonic detection systems are based on surface displacement interferometers. There have been many comprehensive reviews of laser generation of ultrasound in both liquids and solid such as Hutchins [106], Sigrist *et al.* [107,108], Lyamshev *et al.* [109,110] and Scruby *et al.* [111]. Monchalin [112] and Scruby *et al.* [111] have also presented reviews of laser detection of ultrasound.

#### 3.4.1 Laser Generation of Ultrasound

Many physical processes occur when a surface is illuminated by a laser, including heating, generation of thermal waves, generation of elastic waves (ultrasound), and material may be ablated from the surface and a plasma formed. However our focus is the generation of elastic waves from laser illumination. Numerous mechanisms have been recognized as contributing factors to laser generation in both liquids and solids; including thermoelastic expansion, ablation (vaporization), surface melting, plasma formation, dielectric breakdown, electrostriction and radiation pressure [111]. However, the two dominant mechanisms for ultrasonic generation are thermoelastic expansion and ablation.

At low laser power densities ( $<10^6$  W/cm<sup>2</sup>) localized heating in the region of irradiation produces an elastic pulse by thermal expansion of the heated volume, Fig. 3.8(a). This thermoelastic expansion generates relatively strong forces parallel to the surface and a weak force normal to the surface, from thermal diffusion, thereby generating both longitudinal and shear waves.

At higher power densities ( $>10^8$  W/cm<sup>2</sup>) the incident laser pulse raises the surface temperature above the vaporization threshold and a small region of material is ablated, Fig. 3.8(b). During ablation, or vaporization in the case of liquids, atoms and small droplets are ejected from the surface at high velocities creating a transient force normal to the surface and a large amplitude elastic impulse directed normal to the sample. This generates a strong longitudinal pulse normal to the surface. During ablation, the thermoelastic stresses, which would always accompany ablation, are negligible compared to the forces generated from ablation. Therefore, it would seem that ablation would be necessary to produce longitudinal waves of significant amplitude for non-destructive testing applications in applications where some surface damage is allowable.

However, large amplitude longitudinal waves are also generated during thermoelastic expansion if the surface is constrained with a thin layer of liquid between a transparent solid and the sample surface. This technique modifies the surface of the sample to introduce large stresses normal to the surface, which are otherwise minimal for the thermoelastic source at a free surface by three mechanisms; constraint of the solid, thermoelastic expansion of the liquid and constraint of the liquid itself. Thus the constrained surface source generates a sound field more akin to that of ablation, but at significantly lower power densities and with minimal surface damage. However, the need to constrain a surface in this manner reduces the usefulness of the laser ultrasonic source for many non-destructive testing applications.

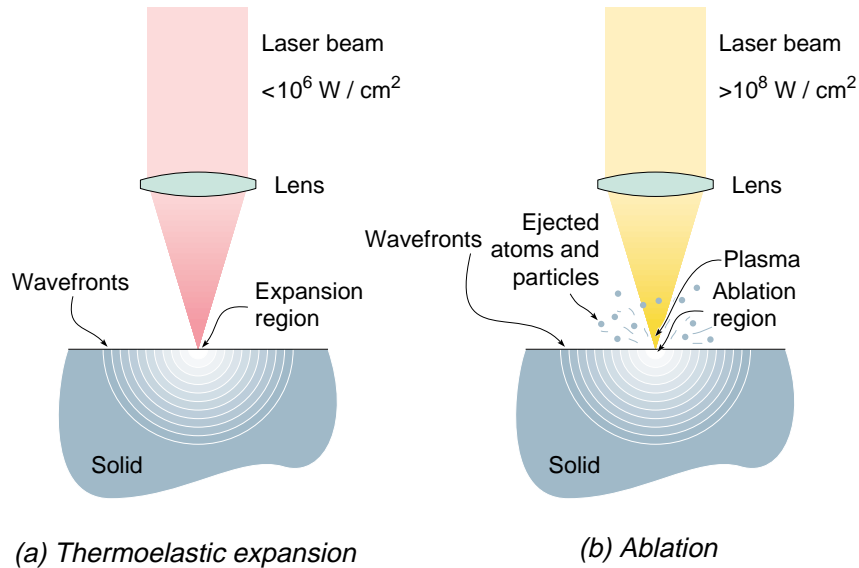


**Figure 3.8** A schematic illustration showing generation mechanisms incurred during laser generation; (a) thermoelastic expansion and (b) ablation.

### 3.4.2 Laser Detection of Ultrasound

Optical ultrasonic detection systems pose certain advantages over conventional detection systems (piezoelectric and electromagnetic acoustic transducers) in that they are non-perturbing to the crystal growth process. There are a variety of optical detection systems which can be employed for the detection of ultrasound; the knife edge technique, surface displacement interferometry and velocity interferometry [112]. Although laser interferometry is rather insensitive compared with piezoelectric devices, it offers a number of advantages including; easily translatable, no fundamental restriction on surface temperature, high spatial resolution and measurements may be localized over a few microns.

The optical detection of ultrasound can be accomplished interferometrically by collecting the light reflected (or scattered) from a surface as it is subjected to an ultrasonic disturbance, Fig. 3.9. Surface displacement interferometers interfere the scattered/reflected light with a reference beam resulting in a measurement of the optical phase

which is directly related to the instantaneous surface displacement. Most optical ultrasonic detection systems are based on surface displacement interferometers such as the Michelson or Mach-Zehnder type interferometer. The Mach-Zehnder heterodyne interferometer (as used here) uses a two beam system in which a single laser beam is split and frequency shifted (via a Bragg cell). In velocity interferometry, changes in the frequency of the scattered or reflected light are monitored and the doppler shift is used to measure velocity. Surface displacement interferometers (Michelson or Mach-Zehnder) are widely used at low frequencies with highly reflective surfaces whereas velocity interferometers offer higher sensitivities at high frequencies and do not require highly reflective surfaces.

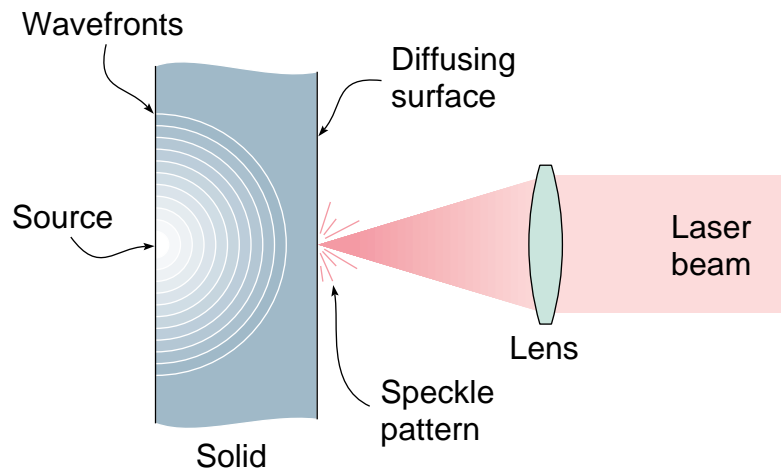


**Figure 3.9** A schematic illustration showing optical detection via interferometry.